

Exploration and inference in spatial extremes using empirical basis functions

Samuel A. Morris¹, Brian J. Reich¹ and Emeric Thibaud²

Abstract

Statistical methods for inference on spatial extremes of large datasets are yet to be developed. Motivated by standard dimension reduction techniques used in spatial statistics, we propose an approach based on empirical basis functions to explore and model spatial extremal dependence. Based on a low-rank max-stable model we propose a data-driven approach to estimate meaningful basis functions using empirical pairwise extremal coefficients. These spatial empirical basis functions can be used to visualize the main trends in extremal dependence. In addition to exploratory analysis, we describe how these functions can be used in a Bayesian hierarchical model to model spatial extremes of large datasets. We illustrate our methods on extreme precipitations in eastern U.S.

Keywords: Dimension reduction; Max-stable process; Non-stationary data analysis

¹North Carolina State University

²Ecole Polytechnique Fédérale de Lausanne

1 Introduction

The spatial extreme value analysis (EVA) literature is expanding rapidly (see, e.g., [Davison et al., 2012, 2013](#); [Dey and Yan, 2015](#)) to meet the demands of researchers to improve estimates of rare-event probabilities by borrowing information across space and to estimate the probability of extreme events occurring simultaneously at multiple locations. Environmental datasets commonly include observations from hundreds or thousands of locations, and advanced tools are required to explore and analyze these data. For Gaussian data, Principle Components Analysis (PCA, [Everitt and Hothorn, 2008](#)), also known as Empirically Orthogonal Functions (EOFs, [Hannachi et al., 2007](#)), has proven to be a powerful tool to study correlation between spatial locations; understand the most important large-scale spatial features; and reduce the dimension of the problem to allow for simple computation even for massive datasets. Computation and exploration are arguably more difficult for EVA than Gaussian data, yet to our knowledge no tool analogous to spatial PCA has been developed for EVA. [Bernard et al. \(2013\)](#) proposed a clustering method for spatial extremes, which can be interpreted as a dimension reduction method; our approach is different and is motivated by identifying drivers of spatial extremes much like PCA and EOF approaches do.

In EVA, extremes are separated from the bulk of the distribution by either analyzing only points above a threshold or block maxima ([Coles, 2001](#)), e.g., the daily precipitation values exceeding a high threshold or their annual maxima. A natural spatial model for block maxima at several spatial locations is the max-stable process, which, under certain conditions, arises as the limit of the location-wise linearly scaled pointwise maxima of infinitely-many spatial processes ([de Haan and Ferreira, 2006](#), Chapter 9). Max-stable processes can also be used to model spatial exceedances over a high threshold ([Thibaud et al., 2013](#); [Huser and Davison, 2014](#)).

Inference for max-stable models is challenging because their likelihoods are intractable in large dimensions. [Padoan et al. \(2010\)](#) proposed the use of composite likelihoods for estimating parameters of max-stable models. More efficient approaches based on full likelihoods were recently developed for extremal threshold exceedances models ([Wadsworth and Tawn, 2014](#); [Engelke et al., 2015](#); [Thibaud and Opitz, 2015](#)) but these do not apply for max-stable models fitted to block max-

ima. Alternatively, non-max-stable models that retain extremal dependence such as the skew- t process of [Morris et al. \(2017\)](#) can be used for extremes. [Thibaud et al. \(2016\)](#) showed how fully-Bayesian analysis can be performed for max-stable models, but the approach is cumbersome for large data sets. [Reich and Shaby \(2012\)](#) proposed a Bayesian max-stable model, based on a low-rank method based on spatial kernel functions. Although the previous model can be fit to large datasets, the Bayesian inference is computationally intensive. In this paper we will build on the previous model and show how the inference can be improved by considering a data-based low-rank approximation of the max-stable process.

The spectral representation ([de Haan and Ferreira, 2006](#), §9.6) states that any max-stable process can be represented in terms of a countable number of spatial processes, for example using Gaussian processes ([Schlather, 2002](#)) or log Gaussian processes ([Kabluchko et al., 2009](#)). In this paper we propose an empirical basis function (EBF) approach that builds on a finite truncation of the spectral representation of max-stable process, as in [Wang and Stoev \(2011\)](#), and develops a method-of-moments estimator for the underlying spatial processes. Unlike PCA/EOFs, but similar to dictionary learning ([Mairal et al., 2014](#)) and non-negative matrix factorizations ([Lee and Seung, 1999](#)), the EBFs are not orthogonal. Nonetheless these spatial functions can be plotted for exploratory analysis to reveal important spatial trends. In addition to exploratory analysis, we describe how the EBFs can be used for Bayesian inference. By basing the spatial dependence on EBFs, the resulting spatial analysis does not require dubious assumptions such as stationarity. In addition, a Bayesian analysis for either block-maxima or point above a threshold is computationally feasible for large datasets because the entire spatial process is represented by a small number of basis functions.

The paper proceeds as follows. In [Section 2](#) we present the low-rank model. [Section 3](#) describes the algorithm used to estimate the spatial basis functions, and [Section 4](#) describes the use of EBFs in a Bayesian hierarchical model. In [Section 5](#) we present the results of a simulation study to evaluate the performance of our method for estimating basis functions. In [Section 6](#) we demonstrate the use of the EBFs for an analysis of precipitation data in the eastern U.S. Lastly in

Section 7 we give some summary conclusions and a brief discussion of the findings.

2 Low-rank max-stable model

Let $Y_t(\mathbf{s})$ be the observation process at spatial location $\mathbf{s} \in \mathcal{S}$ and time t ; \mathcal{S} is a compact set in \mathbb{R}^2 . We temporarily drop the subscript t and describe the model for the process $Y(\mathbf{s})$ for a single time point, but return to the spatiotemporal notation in Section 3.

Spatial dependence is captured by modeling $Y(\mathbf{s})$ as a max-stable process. Max-stable processes have generalized extreme value (GEV) marginal distributions. At each location $\mathbf{s} \in \mathcal{S}$ the GEV distribution is

$$F_{\mathbf{s}}(y) = \Pr\{Y(\mathbf{s}) \leq y\} = \exp\left(-\left[1 + \xi(\mathbf{s}) \left\{\frac{y - \mu(\mathbf{s})}{\sigma(\mathbf{s})}\right\}\right]_+^{-1/\xi(\mathbf{s})}\right), \quad (1)$$

where $x_+ = \max(0, x)$. This distribution is denoted $\text{GEV}\{\mu(\mathbf{s}), \sigma(\mathbf{s}), \xi(\mathbf{s})\}$ and has three real parameters: location $\mu(\mathbf{s})$, scale $\sigma(\mathbf{s}) > 0$ and shape $\xi(\mathbf{s})$; the case $\xi(\mathbf{s}) = 0$ is defined as a limit in (1). Spatial dependence is present both in the GEV parameters and in the standardized residual process $Z(\mathbf{s}) = -[\log F_{\mathbf{s}}\{Y(\mathbf{s})\}]^{-1}$ which is max-stable and has unit Fréchet, i.e., $\text{GEV}(1,1,1)$, marginal distribution for all \mathbf{s} .

Our objective is to identify a low-rank max-stable model for the spatial dependence of the residual process $Z(\mathbf{s})$. The spectral representation discussed in [de Haan and Ferreira \(2006, Theorem 9.6.1\)](#) shows that any max-stable process $Z(\mathbf{s})$ with unit Fréchet margins and continuous sample paths can be written as

$$Z(\mathbf{s}) = \max_{l=1,2,\dots} B(\mathbf{s}, \mathbf{k}_l) q_l, \quad (2)$$

where the functions $B(\mathbf{s}, \mathbf{k}_l)$ are nonnegative and satisfy $\int B(\mathbf{s}, \mathbf{k}_l) d\mathbf{k}_l = 1$ for all $\mathbf{s} \in \mathcal{S}$, and $\int \sup_{\mathbf{s} \in \mathcal{S}} B(\mathbf{s}, \mathbf{k}_l) d\mathbf{k}_l < \infty$, and $(\mathbf{k}_1, q_1), (\mathbf{k}_2, q_2), \dots$ are the points of a Poisson process with intensity measure $d\mathbf{k} \times (dq/q^2)$ on $\mathcal{S} \times (0, \infty)$. Conversely, a max-stable process with unit Fréchet marginals is obtained by choosing particular functions $B(\mathbf{s}, \mathbf{k}_l)$ satisfying the conditions stated above ([de Haan and Ferreira, 2006, Theorem 9.6.1](#)); this has been used to construct max-stable

models (e.g., [Smith, 1990](#); [Schlather, 2002](#); [Kablichko et al., 2009](#)). In several max-stable models, such as [Smith \(1990\)](#) and [Reich and Shaby \(2012\)](#), the \mathbf{k}_l are spatial locations that represent the center of process $B(\mathbf{s}, \mathbf{k}_l)$; however, in our proposed method the basis functions are not associated with one particular location and so to simplify notation we let $B_l(\mathbf{s}) = B(\mathbf{s}, \mathbf{k}_l)$.

To arrive at a low-rank model, we assume that there is a finite and known number L of spatial basis functions $B_1(\mathbf{s}), \dots, B_L(\mathbf{s})$ that explain the important spatial variation in the process. We motivate our approach as follows. [Smith \(1990\)](#) uses the physical analogy that in (2), \mathbf{k}_l is storm l 's spatial center, $B(\mathbf{s}, \mathbf{k}_l)$ is the storm's spatial extent, and q_l is the magnitude of its precipitation. The response $Z(\mathbf{s})$ is thus the maximum of the precipitation over the year's storms at site \mathbf{s} . Following this analogy, our dimension reduction approach identifies the L most influential storm patterns, $B_1(\mathbf{s}), \dots, B_L(\mathbf{s})$, and expresses year-to-year variation in terms of the annual intensity of these L storm patterns.

Assuming a finite number L of basis function we can rearrange (2) to write

$$Z(\mathbf{s}) = \max_{l=1, \dots, L} B_l(\mathbf{s})Z_l, \quad (3)$$

where Z_1, \dots, Z_L are unit Fréchet random variables and the nonnegative basis functions are restricted so that $\sum_{l=1}^L B_l(\mathbf{s}) = 1$ for all \mathbf{s} . Model (3) is known as a max-linear process. It can be shown that any max-stable process can be arbitrary well approximated by a low-rank max-linear model for some suitable choice of basis functions. This approximation was used by [Wang and Stoev \(2011\)](#) to obtain approximate conditional simulations from max-stable models.

Because it is unrealistic to assume that extreme realizations are exactly functions of L basis functions, the process (3) is inappropriate for modeling complex data based on a small number L of basis functions. Hence we use a different low-rank max-stable model proposed by [Reich and Shaby \(2012\)](#), which is based on multivariate max-stable models from [Fougères et al. \(2009\)](#) and [Fougères et al. \(2013\)](#), and which can be seen as a noisy version of model (3). We consider the model

$$Z(\mathbf{s}) = \theta(\mathbf{s})\epsilon(\mathbf{s}) \quad \text{where} \quad \theta(\mathbf{s}) = \left\{ \sum_{l=1}^L B_l(\mathbf{s})^{1/\alpha} A_l \right\}^\alpha, \quad (4)$$

and where $\varepsilon(\mathbf{s}) \stackrel{\text{iid}}{\sim} \text{GEV}(1, \alpha, \alpha)$, $B_l(\mathbf{s}) \geq 0$, $\sum_{l=1}^L B_l(\mathbf{s}) = 1$ for all \mathbf{s} , and the A_l have positive stable (PS; Appendix A.1) distribution, $A_l \stackrel{\text{iid}}{\sim} \text{PS}(\alpha)$, $\alpha \in (0, 1)$; these conditions ensure that $Z(\mathbf{s})$ is max-stable and has unit Fréchet marginal distributions. The functions $B_l(\mathbf{s})$ control the shape of spatial dependence in the process $Z(\mathbf{s})$ while the parameter α acts as a nugget effect introducing independent noise at each location \mathbf{s} and thus giving discontinuous realizations of $Z(\mathbf{s})$. Reich and Shaby (2012, Fig. 1) shows the effects of the basis functions and α on realizations of $Z(\mathbf{s})$. As $\alpha \rightarrow 1$ the model converges to independence, i.e., a process with independent unit Fréchet marginals. As $\alpha \rightarrow 0$ multivariate distributions of model (4) converge to those of the max-linear model (3) (Reich and Shaby, 2012, Section 3).

Reich and Shaby (2012) used standardized Gaussian kernel functions (GKFs) as spatial basis functions in their max-stable model. For $\mathbf{k}_1, \dots, \mathbf{k}_L$ a fixed collection of L spatial knot locations in \mathcal{S} , they defined

$$B_l(\mathbf{s}) = \frac{\exp\{-\|\mathbf{s} - \mathbf{k}_l\|/\rho\}^2}{\sum_{j=1}^L \exp\{-\|\mathbf{s} - \mathbf{k}_j\|/\rho\}^2}, \quad (5)$$

where $\|\cdot\|$ is the Euclidean norm and $\rho > 0$ is a bandwidth parameter that they estimated as part of their Bayesian model. For a large and dense grid of knots $\mathbf{k}_1, \dots, \mathbf{k}_L$ the GKF model provides a good approximation to the max-stable model of Smith (1990). In this paper, rather than selecting a predefined form for the basis functions B_l we will estimate them from the data.

Extremal spatial dependence for max-stable processes can be summarized by the pairwise extremal coefficient $\vartheta(\mathbf{s}_1, \mathbf{s}_2) \in [1, 2]$ defined such that

$$\Pr\{Z(\mathbf{s}_1) \leq z, Z(\mathbf{s}_2) \leq z\} = \Pr\{Z(\mathbf{s}_1) \leq z\}^{\vartheta(\mathbf{s}_1, \mathbf{s}_2)},$$

with $\vartheta(\mathbf{s}_1, \mathbf{s}_2) = 1$ and $\vartheta(\mathbf{s}_1, \mathbf{s}_2) = 2$ corresponding to perfect dependence and independence of $Z(\mathbf{s}_1)$ and $Z(\mathbf{s}_2)$ respectively. For the positive stable random effects model (4) it can be shown that the extremal coefficient for $\mathbf{s}_1 \neq \mathbf{s}_2$ is

$$\vartheta(\mathbf{s}_1, \mathbf{s}_2) = \sum_{l=1}^L \{B_l(\mathbf{s}_1)^{1/\alpha} + B_l(\mathbf{s}_2)^{1/\alpha}\}^\alpha.$$

In particular, $\lim_{\|\mathbf{s}_1 - \mathbf{s}_2\| \rightarrow 0} \vartheta(\mathbf{s}_1, \mathbf{s}_2) = 2^\alpha$, showing how α can be interpreted as a nugget effect in the model, as creating a discontinuity in the extremal coefficient function; note that $\vartheta(\mathbf{s}, \mathbf{s}) = 1$ by definition.

In the next sections we will explore and model residual dependence in the process $Y(\mathbf{s})$ using model (4). The motivation for our approach is that model (4) can be used as an approximation to most max-stable processes for a sufficiently large number L of basis functions $B_l(\mathbf{s})$ suitably chosen. The functions $B_l(\mathbf{s})$ represents the main trends in the max-stable process $Z(\mathbf{s})$. We propose to estimate these basis functions, so-called empirical basis functions (EBFs), using extremal coefficients and then show how inference for $Y(\mathbf{s})$ can be based on these EBFs.

3 Estimating the basis functions

We describe the estimation of the EBFs for model (4) using pairwise extremal coefficients. To estimate the extremal coefficient function, we consider the process at n_s spatial locations $\mathbf{s}_1, \dots, \mathbf{s}_{n_s}$ and n_t times $t = 1, \dots, n_t$. The basis functions are fixed over time, but the random effects and errors are independent over time. That is

$$Z_t(\mathbf{s}) = \theta_t(\mathbf{s})\epsilon_t(\mathbf{s}) \quad \text{where} \quad \theta_t(\mathbf{s}) = \left\{ \sum_{l=1}^L B_l(\mathbf{s})^{1/\alpha} A_{lt} \right\}^\alpha, \quad (6)$$

$A_{lt} \stackrel{\text{iid}}{\sim} \text{PS}(\alpha)$, and $\epsilon_t(\mathbf{s}) \stackrel{\text{iid}}{\sim} \text{GEV}(1, \alpha, \alpha)$. Denote $Y_t(\mathbf{s}_i) = Y_{it}$, $B_l(\mathbf{s}_i) = B_{il}$ and $\vartheta(\mathbf{s}_i, \mathbf{s}_j) = \vartheta_{ij}$.

In this section we develop an algorithm to estimate the parameter α and the $n_s \times L$ matrix $\mathbf{B} = \{B_{il}\}$. Our algorithm has the following steps:

1. Obtain an initial empirical estimate of the extremal coefficient for each pair of locations, $\hat{\vartheta}_{ij}$.
2. Spatially smooth the $\hat{\vartheta}_{ij}$ using kernel smoothing to obtain $\tilde{\vartheta}_{ij}$.
3. Estimate the spatial dependence parameters by minimizing the distance between model-based coefficients ϑ_{ij} and smoothed empirical coefficients $\tilde{\vartheta}_{ij}$.

The first-stage empirical estimates $\hat{\vartheta}_{ij}$ of the extremal coefficients are obtained from the F-madogram estimator of [Cooley et al. \(2006\)](#), using the ‘SpatialExtremes’ ([Ribatet, 2015](#)) package

of R (R Core Team, 2016); see Appendix A.2 for the definition of the estimator. Note that other estimators for $\hat{\vartheta}_{ij}$ could be used, such as the estimators of Smith (1990) or Schlather and Tawn (2003). Assuming the true extremal coefficient is smooth over space, the initial estimates $\hat{\vartheta}_{ij}$ can be improved by smoothing. For $i \neq j$ let

$$\tilde{\vartheta}_{ij} = \frac{\sum_{u=1}^{n_s} \sum_{v=1}^{n_s} w_{iu} w_{jv} \hat{\vartheta}_{uv}}{\sum_{u=1}^{n_s} \sum_{v=1}^{n_s} w_{iu} w_{jv}}, \quad (7)$$

where $w_{iu} = \exp\{-\|\mathbf{s}_i - \mathbf{s}_u\|/\delta\}^2$ is the Gaussian kernel function with bandwidth $\delta > 0$. The elements $\hat{\vartheta}_{ii}$ deteriorate the estimator $\tilde{\vartheta}_{ij}$ as $\hat{\vartheta}_{ii} = 1$ for all i by construction and because of the possible discontinuity of the extremal coefficient function at the origin. To eliminate this problem we set $w_{ii} = 0$.

First, the parameter α is estimated from the estimates of the extremal coefficients of the closest pairs. For pairs (i, j) corresponding to close spatial locations $(\mathbf{s}_i, \mathbf{s}_j)$ we know $\vartheta_{ij} \approx 2^\alpha$, and therefore we select a set \mathcal{N} of such pairs and use their $\tilde{\vartheta}_{ij}$ to estimate $\hat{\alpha} = \log_2(\sum_{\mathcal{N}} \tilde{\vartheta}_{ij}/|\mathcal{S}|)$. For $\hat{\alpha}$ to be a reasonable estimate of α it is crucial that the data set contains close locations. Second, we estimate \mathbf{B} given $\alpha = \hat{\alpha}$ by minimizing the mean square distance between the estimates $\tilde{\vartheta}_{ij}$ and the model-based extremal coefficients ϑ_{ij} . Similarly to Smith (1990) and Einmahl et al. (2016), we estimate $\hat{\mathbf{B}}$ as the minimizer of the error

$$\sum_{i < j} \left(\tilde{\vartheta}_{ij} - \vartheta_{ij} \right)^2 = \sum_{i < j} \left\{ \tilde{\vartheta}_{ji} - \sum_{l=1}^L \left(B_{il}^{1/\hat{\alpha}} + B_{jl}^{1/\hat{\alpha}} \right)^{\hat{\alpha}} \right\}^2 \quad (8)$$

under the restrictions that $B_{il} \geq 0$ for all i and l , and $\sum_{l=1}^L B_{il} = 1$ for all i . Since the minimizer of (8) does not have a closed form, we use a gradient descent algorithm to obtain $\hat{\mathbf{B}}$. This algorithm gives estimates of the B_{il} at the n_s data locations, but is easily extended to all \mathbf{s} for spatial prediction. The kernel smoothing step ensures that the estimates for \hat{B}_{il} are spatially smooth, and thus interpolation of the \hat{B}_{il} gives spatial functions $\hat{B}_l(\mathbf{s})$.

As mentioned in Section 2, the EBFs provide useful exploratory data analysis techniques. Maps of $\hat{B}_l(\mathbf{s})$ show important spatial features in the extremal dependence. The relative contribution of

each EBF can be measured by

$$v_l = \frac{1}{n_s} \sum_{i=1}^{n_s} \hat{B}_{il}.$$

Since $\sum_{l=1}^L \hat{B}_{il} = 1$ for all i , we have $\sum_{l=1}^L v_l = 1$. Since the EBFs are combined with independent and identically distributed variables A_1, \dots, A_L in (4), the EBFs with largest v_l contribute the most to the model, therefore, EBFs with large v_l are the most important in explaining extreme dependence. The order of the basis functions is arbitrary, so we reorder them so that $v_1 \geq \dots \geq v_L$.

The first-stage estimate of the extremal coefficients has two tuning parameters: the kernel bandwidth (δ) for the smoothing step and the number of basis functions (L). We use cross-validation on the extremal coefficients to choose an appropriate value for δ . For L we can look for an ‘‘elbow’’ in the error (8) to determine a sensible number of basis functions, or we can use a validation data set (or cross-validation) to assess how L affects predictions from the max-stable model, see Section 6.

4 Bayesian modeling based on empirical basis functions

In this section we describe how to use the EBFs to construct a spatial max-stable model for block maxima. The matrix $\hat{\mathbf{B}}$, i.e., the EBFs, and the estimate $\hat{\alpha}$ obtained from the procedure described in Section 3 provide a max-stable model for the residual extremal spatial dependence using the positive stable model (6). Notice that using the EBFs in spatial modeling induces a non-stationary spatial dependence structure. To fully define a max-stable model for block maxima we need to model the marginal GEV distributions in (1). This can be done using space-time models for the marginal GEV parameters, using covariates and Gaussian process priors, as described, for example, in Reich and Shaby (2012). In Section 6 we model only the residual dependence, so we don’t provide more details on marginal modeling in this paper.

The residual dependence parameters $\hat{\mathbf{B}}$ and $\hat{\alpha}$ are fixed and only the positive stable variables A_{lt} and the marginal parameters must be estimated. A nice feature of the hierarchical max-stable model (4) is that conditional on $\theta(\mathbf{s})$, the variables $Y(\mathbf{s})$ are conditionally independent, making Bayesian computations for the marginal parameters relatively easy. All parameters can be esti-

mated using standard MCMC methods, a Metropolis-Hastings algorithm with random walk candidate distributions. The main difficulty in fitting the Bayesian hierarchical model concerns the MCMC algorithm for the positive stable variables A_{lt} . This is because the positive stable density is challenging to evaluate as it does not have a closed form. One technique to avoid this complication is to incorporate auxiliary random variables, see [Stephenson \(2009\)](#) and [Reich and Shaby \(2012\)](#). This approach may lead to poor mixing of the Markov chain of the positive stable variable due to the large number of these auxiliary variables and their dependencies. In [Section 6](#) we use instead a numerical approximation of the positive stable density, see [Appendix A.1](#).

5 Simulation study

In this section we conduct a simulation study to evaluate the performance of our method for estimating the EBFs. Each data set consists of n_t independent replications of the max-stable process at $n_s = 100$ spatial locations sampled uniformly on $[1, 10] \times [1, 10]$. The data are generated from the [Reich and Shaby \(2012\)](#) model with unit Fréchet marginal distribution, dependence parameter α , and L basis functions $B_{il} = B_l(\mathbf{s}_i)$ defined via [\(5\)](#) with $\rho = 2.5$, where the knots $\mathbf{k}_1, \dots, \mathbf{k}_l$ form a rectangular $\sqrt{L} \times \sqrt{L}$ grid spanning $[1, 10] \times [1, 10]$. We generate 100 data sets for each combination of $L \in \{9, 25\}$, $\alpha \in \{0.3, 0.7\}$, and $n_t \in \{50, 200\}$.

For each data set we compute the EBF estimate of α and the EBF estimate of the basis functions B_{il} using the method of [Section 3](#) with both $L = 9$ and $L = 25$. [Table 1](#) presents the mean and standard deviation of the estimates of α over the 100 data sets. We also compute the mean squared error for estimating the true extremal coefficients ϑ_{ij} (determined by the true α and B_{il}) averaged over i, j and the 100 datasets. We compare four estimators of the extremal coefficients: (1) the initial estimates from the F-madogram ($\hat{\vartheta}_{ij}$), (2) the smoothed estimates ($\tilde{\vartheta}_{ij}$), (3) the extremal coefficient corresponding to the EBF estimates of α and B_{il} with $L = 9$, (4) the EBF estimates with $L = 25$.

The EBF method for estimating the spatial dependence parameter α works well in all cases. Smoothing the initial F-madogram estimate leads to an improvement except for the scenario with

Table 1: Simulation study results. The simulation settings vary by the true number of basis functions, L , the spatial-dependence parameter, α , and the number of replicates, n_t . The results for each of the eight scenarios are summarized using the mean (standard deviation) of the EBF estimates of α , and the mean squared error (times 100) of the estimated extremal coefficients ϑ_{ij} for the initial F -madogram estimate, the kernel smoothed estimate, and the EBF estimates assuming $L = 9$ or $L = 25$ basis functions.

Settings			$\hat{\alpha}$	Extremal coefficients			
L	α	n_t		Initial	Smoothed	EBF, $L = 9$	EBF, $L = 25$
9	0.3	50	0.31 (0.02)	1.08	0.87	0.84	0.88
9	0.3	200	0.31 (0.01)	0.28	0.28	0.27	0.31
9	0.7	50	0.70 (0.04)	1.19	0.49	0.50	0.51
9	0.7	200	0.70 (0.02)	0.31	0.14	0.13	0.15
25	0.3	50	0.32 (0.02)	1.12	0.89	2.08	0.95
25	0.3	200	0.32 (0.01)	0.27	0.29	1.56	0.38
25	0.7	50	0.70 (0.03)	1.12	0.55	0.84	0.60
25	0.7	200	0.70 (0.01)	0.27	0.16	0.46	0.20

strong spatial dependence ($\alpha = 0.3$) and large sample size ($n_t = 200$) where the initial estimate is sufficient. The EBF method with the correct number of basis functions has similar MSE to the smoothed estimate which shows that the method is able to efficiently represent spatial dependence with a small number of basis functions. As expected, MSE increases slightly when too many basis functions are included (the first four rows of Table 1), and MSE increases substantially when too few basis functions are included (the final four rows of Table 1). This suggests that the user should error on the side of including too many basis functions.

6 Analysis of annual maximum precipitations

We illustrate the EBF method with an analysis of annual maxima of precipitation in the eastern U.S. We use the same dataset as Reich and Shaby (2012) and we compare our EBF approach to their original Gaussian kernel function (GKF) approach. The data are climate model output from the North American Regional Climate Change Assessment Program (NARCCAP). This dataset consists of $n_s = 697$ grid cells at a 50 km resolution in the eastern US, and includes historical data (1969–2000) as well as future conditions (2039–2070).

We focus on the analysis of the residual dependence in the data and in particular in comparing

our EBF method with the original GKF method in terms of dependence modeling. In order to focus on the residual dependence we transformed the data to common unit Fréchet marginals in a first step, and then performed all subsequent analysis on the unit Fréchet scale assuming the marginals are fixed and known exactly. This was done to isolate differences in residual dependence modeling, which is the focus of the current paper. Initial data analysis on the transformed data suggests that the dependence is different between current and future periods. The residual extreme dependence appear stronger in the future period than in the current period. Thus we decided to analyze the two periods separately.

We compare the proposed EBF method described in Sections 2-4 with the Gaussian kernel functions (GKFs) model of Reich and Shaby (2012). Reich and Shaby (2012) fit a model that uses standardized Gaussian kernel functions (GKFs), see (5), centered on a set of $\mathbf{k}_1, \dots, \mathbf{k}_L$ spatial knots for the spatial basis functions $B_l(\mathbf{s})$. We denote by ρ the bandwidth of these Gaussian kernels. To compare the EBF and GKF methods we apply two modifications to the original GKF approach. First, Reich and Shaby (2012) used a large number of GKF, but here we use a relatively small number L of basis functions for both EBF and GKF approaches. The spatial knots $\mathbf{k}_1, \dots, \mathbf{k}_L$ are selected using the ‘cover.design’ function in the ‘fields’ (Nychka et al., 2015) package of R, with default settings; the method selects the centroid locations which minimize a geometric space-filling criterion. Second, Reich and Shaby (2012) estimated ρ and α in the MCMC algorithm, but here we use the procedure described in Section 3 to estimate the dependence parameters for both methods and then treat these parameters as fixed in the MCMC algorithm. In particular, $\hat{\alpha}$ is the same for the EBF and GKF methods and does not depend on L .

6.1 Comparison of EBF and GKF methods

The analysis of the transformed data (which we called the residuals) is performed in two steps: first we estimate α , the EBFs, and the GKFs bandwidth ρ as described in Section 3, and second we fit Bayesian hierarchical models based on these basis functions as described in Section 4, with marginals that are fixed to unit Fréchet; i.e., the MCMC algorithm only estimates the latent

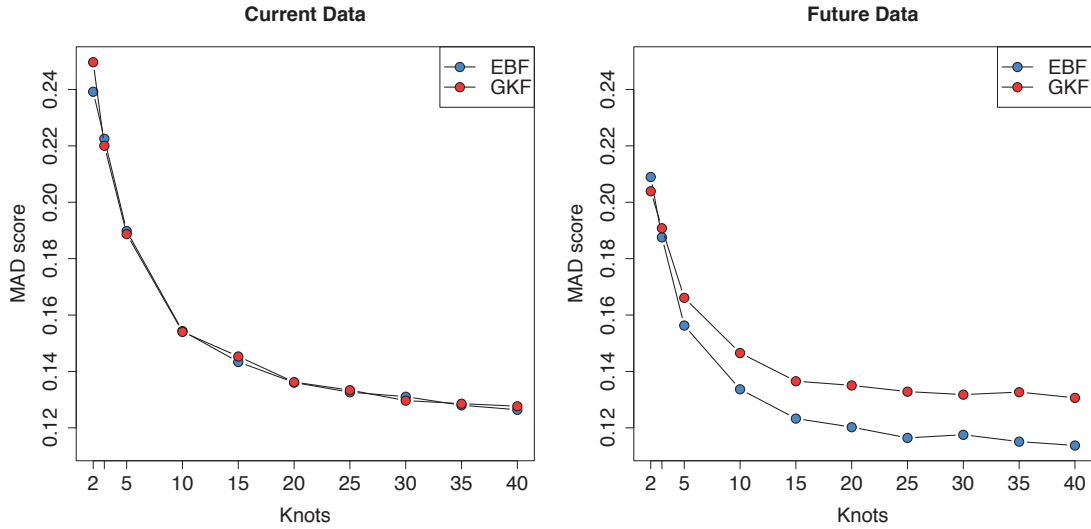


Figure 1: Mean absolute deviation (MAD) scores by the number of basis functions (L) estimated using cross-validation. Current and future data are modeled and evaluated separately.

variables A_{lt} . We apply these methods to the two periods separately.

We use 5-fold cross-validation to assess the predictive performance of the EBF and GKF models for current and future data and for different values of L . The dataset is randomly split into five (roughly-equal size) parts across sites and years. The models are then trained onto observations of four of the five parts and the remaining observations are used to evaluate the predictions. Training the models imply estimating α , the EBF and the GKF and then using the MCMC to predict data on the test set. To assess the predictions for the test set we use the mean absolute deviation (MAD). The two periods are treated separately in terms of fit and evaluation. The scores for the current and future precipitation data analysis are given in Figure 1.

We observe some variation in the scores across the number of basis functions L . On the current data, EBF and GKF method give similar results (scores are only significantly different for $L = 2$). The MAD score reduces sharply from $L = 2$ to $L = 10$, and only slightly after $L = 30$. On the future data, EBF gives lower MAD score than GKF for all L . The MAD score reduces sharply from $L = 2$ to $L = 10$, and seems to stabilize around $L = 15$. These results suggest that 10 EBFs might be sufficient to adequately model spatial dependence in current and future precipitation data.

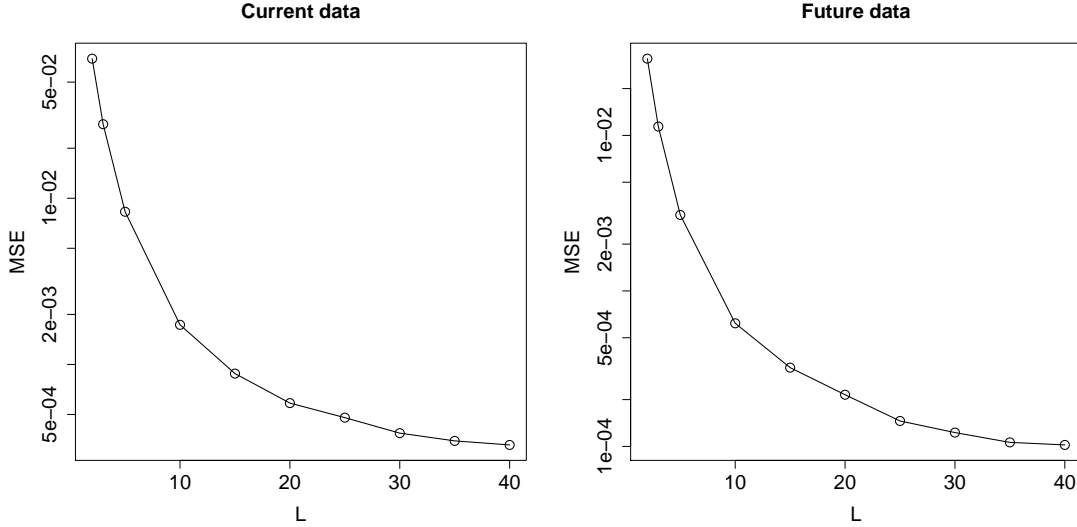


Figure 2: Mean squared error (proportional to (8)) of EBFs by the number of basis functions (L). Note the y-axis is on log scale.

6.2 Extremal dependence in current and future precipitations

In this section we discuss the analysis of all current and future data; again the two periods are analyzed separately. The cross-validation results suggest using $L = 10$ for both current and future data. As an alternative method to choose L we estimated the EBFs for various values of L and we computed the error (8) between the smoothed empirical extremal coefficients and the EBF based extremal coefficients, see Figure 2. This plot also suggests that $L = 10$ is a reasonable choice for both periods, without the need of extensive modeling fitting.

We discuss the EBFs for $L = 10$ for current and future data. First, for current data $\hat{\alpha} = 0.24$, and for future data $\hat{\alpha} = 0.21$, showing the residuals are smoother for the future period. The first six EBFs (out of ten) along with their contributions v_1, \dots, v_6 are given in Figure 3 for current data, and in Figure 4 for future data. These six EBFs show the main features needed to reconstruct extremal dependence in the annual maximum precipitations in this region. Most of the EBFs capture local features. For example, the first EBF for the current regime explains extreme precipitation in the Appalachian Mountains, while the second separates the south from the rest of the spatial domain.

Figures 5 and 6 show extremal coefficient maps $\{\vartheta(\mathbf{s}_i, \mathbf{s})\}_{\mathbf{s} \in \mathcal{S}}$ for some sites \mathbf{s}_i . The estimates

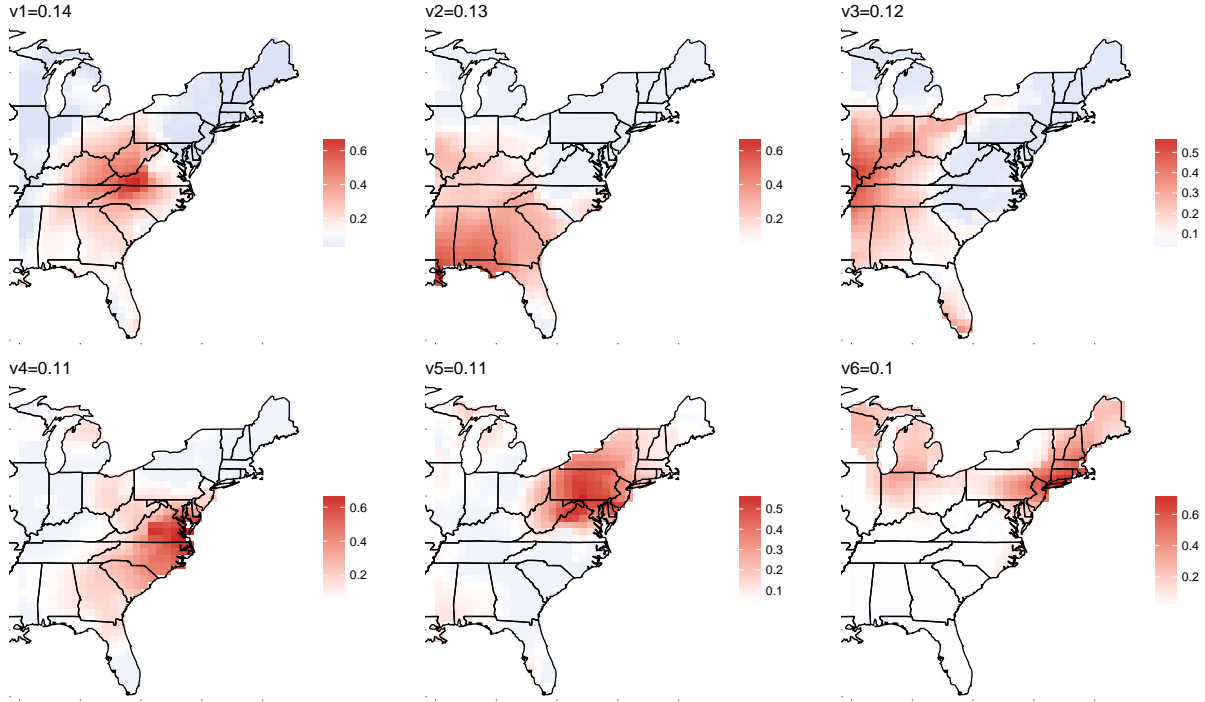


Figure 3: First six EBFs along with their contributions v_1, \dots, v_6 , for $L = 10$ and for the current precipitation data. Note the different scales in each figure.

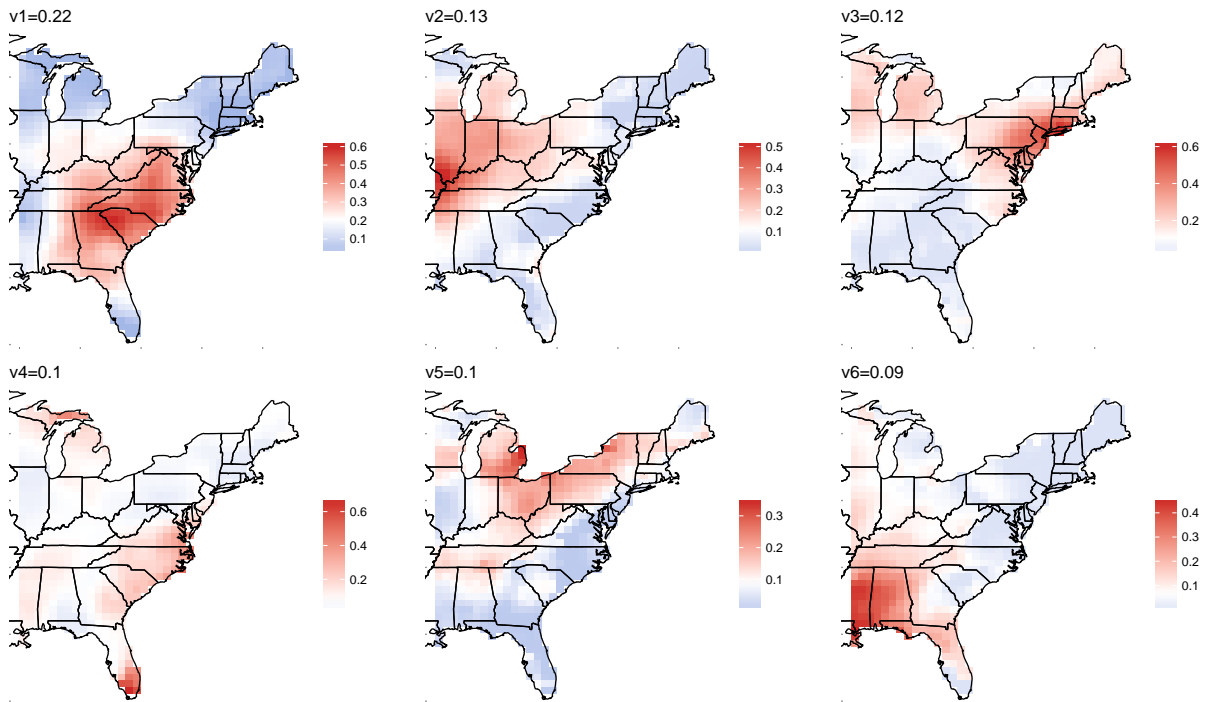


Figure 4: First six EBFs along with their contributions v_1, \dots, v_6 , for $L = 10$ and for the future precipitation data. Note the different scales in each figure.

of spatial dependence clearly exhibit non-stationary. For example, in the current climate the range of spatial dependence is much smaller around New York City and Washington, DC than it is around Atlanta and Knoxville. Also, around all four of these cities the range of spatial dependence appears to increase in the future climate.

7 Discussion

In this paper we have proposed a new empirical basis function approach for a data-driven low-rank max-stable process. The EBFs provide researchers with an exploratory data analysis tool to explore spatial extremal dependence. The EBFs can also be used as inputs to a Bayesian model for inference and prediction over space and time.

The results from the data analysis suggest that in the presence of strong spatial dependence, as with the considered future precipitation data, the EBFs show an improvement in prediction accuracy over using the GKF approach. Compared to the original approach of [Reich and Shaby \(2012\)](#) that uses as many kernels as the number of sites, or to [Shaby and Reich \(2012\)](#) and [Stephenson et al. \(2015\)](#) that uses a large number of kernels, centered on a grid or at a subsample of the observation locations, the computation of the Bayesian model based on the EBFs with relatively few basis functions is much faster. On average, it takes 2 seconds for 10000 updates of each latent variable A_{lt} , such that the running time for fitting our EBF dependence model (with fixed marginals) is about $2 \times L \times n_t$ seconds for 10000 iterations of the MCMC algorithm. Cross-validation can be used to select a number of basis functions L such that the predictive accuracy of the Bayesian model using a small number of EBFs is comparable to a more complex Bayesian model using a large number of GKFs.

We have used the EBF for exploratory analysis and Bayesian inference. Another possibility is to use the methods to reduce the data under consideration from the actual responses to loadings A_{lt} . Given the EBFs, one could obtain estimates of the A_{lt} for each time point. Time series of the estimated A_{lt} may be used as a fast and simple method to study large-scale spatiotemporal trends.

The EBF approach introduced here can be easily extended to explore and model extremal de-

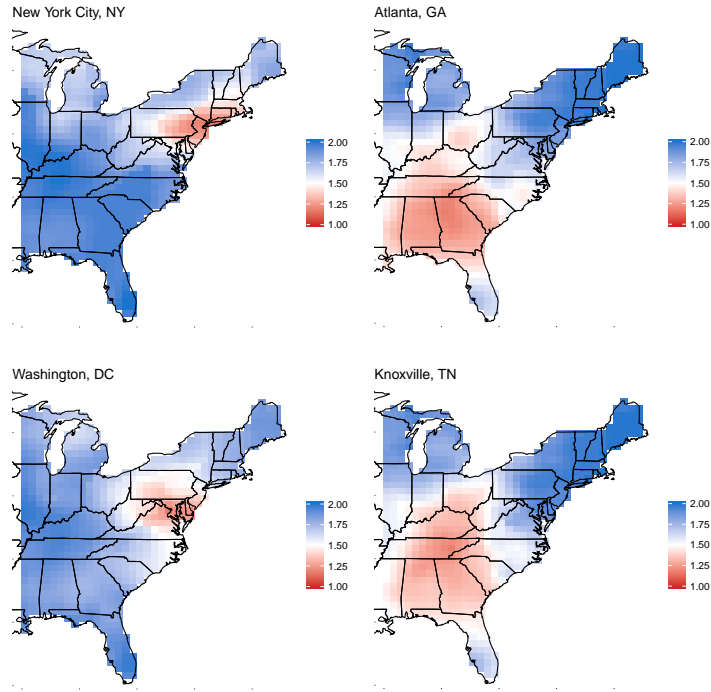


Figure 5: Estimated pairwise extremal coefficients for current data (using $L = 10$) for New York City, NY; Atlanta, GA; Washington, DC; and Knoxville, TN.

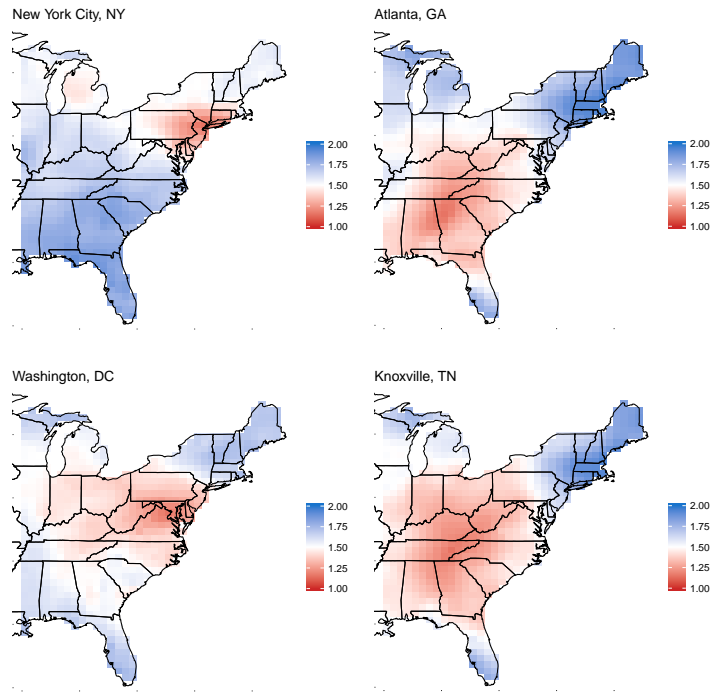


Figure 6: Estimated pairwise extremal coefficients for future data (using $L = 10$) for New York City, NY; Atlanta, GA; Washington, DC; and Knoxville, TN.

pendence in threshold exceedances. Max-stable processes are sensible models for exceedances over large thresholds and empirical extremal coefficients for threshold exceedances can be estimated from censored versions of the likelihood estimator of [Schlather and Tawn \(2003\)](#), for example. From these empirical extremal coefficients, EBFs can be estimated just as described in [Section 3](#). The positive stable max-stable model based on these EBFs can then be fitted to threshold exceedances using a censored approach as in [Reich et al. \(2014\)](#) and [Morris et al. \(2017\)](#).

Acknowledgements

The authors acknowledge Dan Cooley for his helpful suggestions on the manuscript. The authors' work was partially supported by grants from the Department of the Interior (14-1-04-9), National Institutes of Health (R21ES022795-01A1), the US Environmental Protection Agency (R835228), the National Science Foundation (1107046). The calculations have been performed using the facilities of the Scientific IT and Application Support Center of EPFL.

A Appendix

A.1 Grid approximation to positive stable density

The positive stable density does not have a closed form. From [Stephenson \(2009, Section 2\)](#) the density of $PS(\alpha)$ can be expressed as

$$f(x) = \int_0^1 h(x, y) \, dy, \quad (9)$$

where

$$h(x, y) = \frac{\alpha}{1 - \alpha} \left(\frac{1}{x}\right)^{1/1-\alpha} c(\pi y) \exp \left\{ -c(\pi y) \left(\frac{1}{x}\right)^{\alpha/(1-\alpha)} \right\},$$

with

$$c(\psi) = \left\{ \frac{\sin(\alpha\psi)}{\sin(\psi)} \right\}^{1/(1-\alpha)} \frac{\sin\{(1 - \alpha)\psi\}}{\sin(\alpha\psi)}.$$

[Stephenson \(2009\)](#) presents an auxiliary variable technique to deal with the integral in the density function, but we opt to numerically evaluate the integral (9) because it is only one-dimensional.

We use the midpoint rule with 50 evenly spaced quantiles of a Beta(0.5, 0.5) distribution as the midpoints.

A.2 F-madogram estimator

For two locations $\mathbf{s}_i, \mathbf{s}_j \in \mathcal{S}$, the F-madogram of [Cooley et al. \(2006\)](#), here defined for a non-stationary max-stable process Y , is

$$\nu^F(\mathbf{s}_i, \mathbf{s}_j) = \frac{1}{2} \mathbb{E} |F_{\mathbf{s}_i}\{Y(\mathbf{s}_i)\} - F_{\mathbf{s}_j}\{Y(\mathbf{s}_j)\}|$$

where $F_{\mathbf{s}_i}$ denote the distribution of $Y(\mathbf{s}_i)$. [Cooley et al. \(2006\)](#) showed the extremal coefficient is related to the F-madogram by $\vartheta(\mathbf{s}_1, \mathbf{s}_2) = \{1 + 2\nu^F(\mathbf{s}_i, \mathbf{s}_j)\} / \{1 - 2\nu^F(\mathbf{s}_i, \mathbf{s}_j)\}$.

Assume we observe n_t realizations y_{i1}, \dots, y_{in_t} of $Y(\mathbf{s}_i)$ at some locations $\mathbf{s}_i \in \mathcal{S}$. We define the nonparametric estimator $\hat{F}_{\mathbf{s}_i}(y_{it}) = \text{rank}(y_{it}) / (n_t + 1)$, where $\text{rank}(y_{it})$ denotes the rank of the value y_{it} among $(y_{i1}, \dots, y_{in_t})$. We estimate the F-madogram by

$$\hat{\nu}^F(\mathbf{s}_i, \mathbf{s}_j) = \frac{1}{2n_t} \sum_{t=1}^{n_t} |\hat{F}_{\mathbf{s}_i}(y_{it}) - \hat{F}_{\mathbf{s}_j}(y_{jt})| = \frac{1}{2n_t} \sum_{t=1}^{n_t} |\text{rank}(y_{it}) / (n_t + 1) - \text{rank}(y_{jt}) / (n_t + 1)|.$$

The extremal coefficient is then estimated by $\hat{\vartheta}(\mathbf{s}_1, \mathbf{s}_2) = \{1 + 2\hat{\nu}^F(\mathbf{s}_i, \mathbf{s}_j)\} / \{1 - 2\hat{\nu}^F(\mathbf{s}_i, \mathbf{s}_j)\}$.

References

- Bernard, E., Naveau, P., Vrac, M., and Mestre, O. (2013). Clustering of Maxima: Spatial Dependencies among Heavy Rainfall in France. *Journal of Climate*, 26(20):7929–7937.
- Coles, S. (2001). *An Introduction to Statistical Modeling of Extreme Values*. Lecture Notes in Control and Information Sciences. Springer, London.
- Cooley, D., Naveau, P., and Poncet, P. (2006). Variograms for spatial max-stable random fields. In Bertail, P., Soulier, P., and Doukhan, P., editors, *Dependence in Probability and Statistics*, volume 187 of *Lecture Notes in Statistics*, chapter Variograms, pages 373–390. Springer New York, New York, NY.

- Davison, A. C., Huser, R., and Thibaud, E. (2013). Geostatistics of Dependent and Asymptotically Independent Extremes. *Mathematical Geosciences*, 45(5):511–529.
- Davison, A. C., Padoan, S. A., and Ribatet, M. (2012). Statistical modeling of spatial extremes. *Statistical Science*, 27(2):161–186.
- de Haan, L. and Ferreira, A. (2006). *Extreme Value Theory: An Introduction*. Springer Series in Operations Research and Financial Engineering. Springer.
- Dey, D. K. and Yan, J. (2015). *Extreme Value Modeling and Risk Analysis: Methods and Applications*. Chapman and Hall/CRC.
- Einmahl, J. H. J., Kiriliouk, A., and Segers, J. (2016). A continuous updating weighted least squares estimator of tail dependence in high dimensions. arXiv:1601.04826.
- Engelke, S., Malinowski, A., Kabluchko, Z., and Schlather, M. (2015). Estimation of Hüsler-Reiss distributions and Brown-Resnick processes. *Journal of the Royal Statistical Society. Series B: Statistical Methodology*, 77:239–265.
- Everitt, B. and Hothorn, T. (2008). Principal components analysis. In *An Introduction to Applied Multivariate Analysis with R*, pages 21–54. Springer New York, New York, NY.
- Fougères, A.-L., Mercadier, C., and Nolan, J. P. (2013). Dense classes of multivariate extreme value distributions. *Journal of Multivariate Analysis*, 116:109–129.
- Fougères, A.-L., Nolan, J. P., and Rootzén, H. (2009). Models for Dependent Extremes Using Stable Mixtures. *Scandinavian Journal of Statistics*, 36(1):42–59.
- Hannachi, A., Jolliffe, I. T., and Stephenson, D. B. (2007). Empirical orthogonal functions and related techniques in atmospheric science: A review. *International Journal of Climatology*, 27(9):1119–1152.
- Huser, R. and Davison, A. C. (2014). Space-time modelling of extreme events. *Journal of the Royal Statistical Society: Series B (Statistical Methodology)*, 76(2):439–461.

- Kabluchko, Z., Schlather, M., and de Haan, L. (2009). Stationary max-stable fields associated to negative definite functions. *Annals of Probability*, 37(5):2042–2065.
- Lee, D. D. and Seung, S. H. (1999). Learning the parts of objects by non-negative matrix factorizations. *Nature*, 401:788 – 791.
- Mairal, J., Bach, F., and Ponce, J. (2014). Sparse modeling for image and vision processing. *Foundations and Trends in Computer Graphics and Vision*, 8:85 – 283.
- Morris, S. A., Reich, B. J., Thibaud, E., and Cooley, D. (2017). A space-time skew- t model for threshold exceedances. *Biometrics*, 73(3):749–758.
- Nychka, D., Furrer, R., and Sain, S. (2015). *fields: Tools for Spatial Data*. R package version 8.2-1.
- Padoan, S. A., Ribatet, M., and Sisson, S. A. (2010). Likelihood-based inference for max-stable processes. *Journal of the American Statistical Association*, 105(489):263–277.
- R Core Team (2016). *R: A Language and Environment for Statistical Computing*. R Foundation for Statistical Computing, Vienna, Austria.
- Reich, B. J. and Shaby, B. A. (2012). A hierarchical max-stable spatial model for extreme precipitation. *The Annals of Applied Statistics*, 6(4):1430–1451.
- Reich, B. J., Shaby, B. A., and Cooley, D. (2014). A Hierarchical Model for Serially-Dependent Extremes: A Study of Heat Waves in the Western US. *Journal of Agricultural, Biological, and Environmental Statistics*, 19(1):119–135.
- Ribatet, M. (2015). *SpatialExtremes: Modelling Spatial Extremes*. R package version 2.0-2.
- Schlather, M. (2002). Models for Stationary Max-Stable Random Fields. *Extremes*, 5(1):33–44.
- Schlather, M. and Tawn, J. A. (2003). A dependence measure for multivariate and spatial extreme values: Properties and inference. *Biometrika*, 90(1):139–156.

- Shaby, B. A. and Reich, B. J. (2012). Bayesian spatial extreme value analysis to assess the changing risk of concurrent high temperatures across large portions of European cropland. *Environmetrics*, 23(8):638–648.
- Smith, R. L. (1990). Max-stable processes and spatial extremes. Unpublished manuscript, University of Surrey, Guildford GU2 5XH, England. <http://www.stat.unc.edu/postscript/rs/spatex.pdf>.
- Stephenson, A. G. (2009). High-dimensional parametric modelling of multivariate extreme events. *Australian & New Zealand Journal of Statistics*, 51(1):77–88.
- Stephenson, A. G., Shaby, B. a., Reich, B. J., and Sullivan, A. L. (2015). Estimating Spatially Varying Severity Thresholds of a Forest Fire Danger Rating System Using Max-Stable Extreme-Event Modeling. *Journal of Applied Meteorology and Climatology*, 54(2):395–407.
- Thibaud, E., Aalto, J., Cooley, D. S., Davison, A. C., and Heikkinen, J. (2016). Bayesian inference for the Brown–Resnick process, with an application to extreme low temperatures. *Annals of Applied Statistics*, 10(4):2303–2324.
- Thibaud, E., Mutzner, R., and Davison, A. C. (2013). Threshold modeling of extreme spatial rainfall. *Water Resources Research*, 49(8):4633–4644.
- Thibaud, E. and Opitz, T. (2015). Efficient inference and simulation for elliptical Pareto processes. *Biometrika*, 102(4):855–870.
- Wadsworth, J. L. and Tawn, J. A. (2014). Efficient inference for spatial extreme value processes associated to log-Gaussian random functions. *Biometrika*, 101(1):1–15.
- Wang, Y. and Stoev, S. A. (2011). Conditional sampling for spectrally discrete max-stable random fields. *Advances in Applied Probability*, 43(2):461–483.